PERGAMON International Journal of Multiphase Flow 26 (2000) 1925–1949

International Journal of Multiphase Flow

www.elsevier.com/locate/ijmulflow

Collision of a vortex with a vaporizing droplet

M. Masoudi*, W.A. Sirignano

Department of Mechanical and Aerospace Engineering, University of California at Irvine, Irvine, CA 92697, USA

Received 13 July 1998; received in revised form 19 October 1999

Abstract

Three-dimensional interactions between an advecting vortex tube and a vaporizing droplet, described by the Navier–Stokes, energy, and species equations, cause fluctuations in the droplet heating and vaporization, manifested by temporal and time-averaged variations in the droplet Nusselt and Sherwood numbers. Stefan flux not only inhibits the droplet heating, it also 'blocks' the influence of vortex collision on the droplet interface inhibiting Nusselt number perturbations. The Stefan flux has a primary effect on the Nusselt number and a secondary one on the Sherwood number. Fluctuations in Sherwood number can be significant in magnitude and exhibit self-similarity in both the temporal and time-averaged response. Derived correlations are demonstrated to be valid for at least three common fuel droplets (*n*-heptane, *n*-octane, *n*-decane). Furthermore, they quantify the effect of vortex collision on the droplet vaporization and compliment the accepted correlations for droplets in axisymmetric flows. It follows that, in spray combustion systems, vortical structures could significantly affect transport mechanisms, vaporization rates, and local mixture ratios.

Keywords: Vortex; Droplet vaporization; Nusselt/Sherwood number; Kolmogorov turbulence

1. Preliminary remarks

It is well-known that droplet heating and vaporization are coupled mechanisms. Vaporization adds a species boundary layer to the momentum and temperature boundary layers. Mass transfer of the fuel vapor from the droplet, which depends on both the vaporization rate and forced convection, involves diffusion through the species boundary layer

* Corresponding author. Present address: Corning Inc., Corning, New York, USA.

0301-9322/00/$ - see front matter
PII: S0301-9322(99)00107-X

and then convection away from the droplet. The mixture molecular weight near the droplet interface is also affected by the fuel vapor. Surface blowing (and the resultant Stefan convection) changes the density near the droplet, decreases the droplet radius in time, and expands the wake region (Chiang, 1990; Chiang et al., 1992). Furthermore, thermophysical properties variations due to temperature and composition creates a two-way coupling between the momentum and temperature equations, and between the momentum and species equations. Therefore, when the non-fluctuating base flow is perturbed, both the thermal and species boundary layers are subject to fluctuations, influencing both the droplet heating and Stefan flux; such is the case when a vortex advects near the droplet.

Sirignano (1983) has presented a critical and detailed overview of droplet vaporization and of spray combustion pertaining to modern theoretical developments, emphasizing that the literature lacks information on vortex–droplet interactions in combustion systems, and arguing that, in turbulent sprays, the largest possible velocity gradients near the droplets would be at the Kolmogorov scale, itself of the order of the droplet size. Order of magnitude estimates are provided there.

Though the literature reveals many details of droplet heating and vaporization in axisymmetric flows (Abramzon and Sirignano, 1987, 1989; Conner and Elghobashi, 1987; Chiang, 1990; Chiang et al., 1992; Niazmand et al., 1994; Shih and Megaridis, 1996), droplet heating and/or vaporization in asymmetric or perturbed flows have received inconsiderable attention. Bellan and Harstad (1991) and Fichot et al. (1994) address a cluster of droplets inside a vortex, but not the miscrostructure variations such as variations in the droplet interfacial mechanisms or in the droplet boundary layers due to the vortex which influence the droplet transport rates.

The interaction between a vortex and a droplet with comparable length-scales has not been widely examined; previous works of this research group investigated variations in the droplet drag coefficient and the induced lift and moment coefficients due to the droplet–vortex interplay (Kim et al., 1995, 1997), then the variations in the convecting heating of a non-vaporizing droplet influenced by vortex collision (Masoudi and Sirignano, 1997, 1998).

In this work, the investigation concentrates on the influence of droplet–vortex collision on the droplet simultaneous heating, vaporization, and mass transfer. Details of the changes in the thermal and species boundary layers are shown. Simultaneous variations in the droplet Nusselt and Sherwood numbers due to the vortex collision are traced in time. Generalized self-similar correlations with the vortex size, strength, circulation, location, and the flow inertia are obtained for a variety of fuel droplets. This work continues previous investigations (Kim et al., 1995, 1997; Masoudi and Sirignano, 1997, 1998) and explores the effect of Kolmogorov scale turbulence on droplet vaporization.

2. Flow description and governing equations

A simplified representation of the flow configuration is shown in Fig. 1. The governing equations, presented below, are formulated under the following assumptions: (1) the flow Mach number is much less than unity, so that dissipation terms may be neglected; (2) gravity and non-inertial terms are small; (3) the droplet Weber number is small so that the droplet remains

spherical; (4) the thermal radiation and Dufour energy flux in the energy equation and the pressure and thermal diffusion in the species equation are negligible; (5) the mixture behaves as an ideal gas; (6) phase equilibrium is maintained at the gas–liquid interphase; (7) liquid-phase thermodynamic properties, except for viscosity and latent heat, are constant; (8) vaporization and mixing with air occur without chemical reactions.

Within a few residence time units after the droplet is injected into the hot gas stream, the external flow field quickly adjusts to the presence of the droplet, and a recirculation zone in the form of a standing vortex ring appears just aft of the droplet (Chiang et al., 1992; Kim et al., 1995). The droplet internal circulation forms due to the shear stresses at its interface.

Initially, the internal temperature of the cold droplet is uniform. The heat received by the droplet goes partly into its vaporization and partly into internal heating. The heat transfer into the droplet is initially dominated by diffusion. With the establishment of the droplet internal circulation, convective heating becomes dominant; finally, reduction of the surface shear stress slows the internal circulation and diffusion again prevails (Chiang, 1990; Chiang et al., 1992).

The mass transport, manifested in the species boundary layer, is affected by both the vaporization rate and the forced convection. Naturally, a 'fast-enough' convection continuously sweeps the fresh vapor at the interface onto the flow mainstream and enhances further vaporization. Vaporization is nevertheless slow in the beginning due to the time needed for the droplet to heat and raise its temperature. Once the surface temperature is high enough, the vaporization rate increases. The flow continuously convects away the generated fuel vapor. The presence of the fuel vapor surrounding the droplet alters the molecular weight of the mixture near the interface. The vaporization also decreases the droplet radius, expands the droplet wake region, and alters the density distribution near the droplet.

For the bi-component (fuel vapor and air) gas phase, the governing equations are the conservation of mass, momentum, energy, and species mass, and the equation of state. For the liquid phase, they are the conservation of mass, momentum, and energy. These equations are nondimensionalized using characteristic scales which are the droplet initial radius, far-upstream flow velocity and temperature, and the gas-phase initial properties; residence time $t \equiv a_0'/U_\infty'$ is the characteristic time, with a and U being the droplet radius and gas free stream velocity, respectively. ($'$ stands for dimensional quantity; subscripts 0 and ∞ represent initial and far upstream quantities, respectively.)

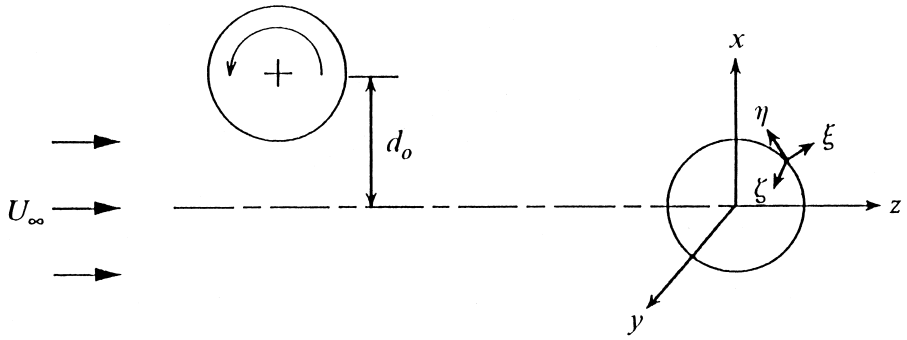

Fig. 1. Flow geometry and coordinates.

2.1. Gas-phase governing equations

$$\frac{\partial \rho_g}{\partial t} + \nabla \cdot \rho_g V_g = 0 \tag{1}$$

$$\rho_g\left[\frac{\partial V_g}{\partial t} + (V_g \cdot \nabla)V_g\right] = -\nabla P_g + \frac{2}{Re_g}\nabla\left[\mu_g \nabla \cdot V_g\right] - \frac{4}{3}\frac{1}{Re_g}\nabla\left[\mu_g \nabla \cdot V_g\right] \tag{2}$$

$$\rho_g C_{p_g}\left[\frac{\partial T_g}{\partial t} + V_g \cdot \nabla T_g\right] + (h_f - h_a)\rho_g\left[\frac{\partial Y_f}{\partial t} + V_g \cdot \nabla Y_f\right] = \frac{2}{Pe_g}\nabla \cdot \left[\kappa_g \nabla T_g\right] + \frac{2}{Pe_m}\nabla \cdot \left[(h_f - h_a)D_g \nabla(\rho_g Y_f)\right] \tag{3}$$

$$\rho_g\left[\frac{\partial Y_i}{\partial t} + V_g \cdot \nabla Y_i\right] = \frac{2}{Pe_m}\nabla \cdot \left[D_g \nabla(\rho_g Y_i)\right] \tag{4}$$

$$P = \frac{\bar{R}}{M}(\rho_g T - M) \tag{5}$$

2.2. Liquid-phase governing equations

$$\nabla \cdot V_l = 0 \tag{6}$$

$$\frac{\partial V_l}{\partial t} + (V_l \cdot \nabla)V_l = -\nabla p_l + \frac{2}{Re_l}\nabla\left[\mu_l \nabla V_l\right] \tag{7}$$

$$\frac{\partial T_l}{\partial t} + V_l \cdot \nabla T_l = \frac{2}{Pe_l}\nabla^2 T_l \tag{8}$$

In the equations above, V, P, T, and Y stand for velocity, pressure, temperature and mass fraction; ρ, μ, C_p, h, κ, D, $\bar{R}$ and M represent density, dynamic viscosity, heat capacity, enthalpy, thermal conductivity, diffusion coefficient, constant of gas law and molecular weight, respectively; Re, Pe and Pr stand for Reynolds, Peclet and Prandtl numbers. Subscripts g, l, f and a stand for gas, liquid, fuel and air properties, respectively, and Pe_m is Peclet number for gas-phase mass transport. i in Eq. (4), the species equation, is for species — fuel vapor or air.

2.3. Gas–liquid interface conditions

The conditions at the interface are the continuity of shear stresses, continuity of tangential velocities, continuity of temperature, energy balance (including the latent heat of vaporization), species mass balance, and thermodynamic equilibrium (Clasius–Clapeyron equation). Since the interface in our flow is always spherical (under the assumption of small Weber number), these conditions are conveniently cast in terms of spherical coordinates (r, θ, ϕ) with the origin placed at the center of the droplet. τ_l, $r\theta$, $i=\tau_g$, $r\theta$, i; τ_l, $r\phi$, $i=\tau_g$, $r\phi$, i; V_l, θ, $i=V_g$, θ, i; V_l, ϕ, $i=V_g$, ϕ, i; T_l, $i=T_g$, i; $q''_{l,\,i}+q''_{lat,\,i}=q''_{g,\,i}$; $(D_g\frac{\partial Y_f}{\partial r})_i=[V_g,\ r(Y_f-1)]_i$; and $P'_f=\exp(c_1-c_2/T_{g,\,i})$. Here, i stands for interface and τ and q'' represent shear stress and heat flux, respectively, with $q''_{lat,\,i}$ being the latent heat of vaporization at the interface. $\tau_{r\theta,\,i}$ and $\tau_{r\phi,\,i}$ are respectively the shear stresses on a positive r-plane in the positive θ and ϕ directions. The interface condition for pressure is obtained from the momentum equation; thermocapillary forces have been also included in the balance equations for the shear stresses due to surface temperature variation over the droplet at the interface inducing Marangoni effects (Niazmand et al., 1994; Shih and Megaridis, 1996).

2.4. Gas-phase boundary conditions

(N_1, N_2, N_3) and (N_{1l}, N_2, N_3) are the number of grid points in the gas phase and the liquid domain, respectively, in (ξ, η, ζ) computational coordinates, shown in Fig. 1. ξ at N_{1l} and N_1 are the droplet surface and the gas far-field, respectively. The far-field quantities for the inflow (imposed upstream at $\xi=N_1$, $N_{2\,mid}\le\eta\le N_2$; i.e. at $\pi/2\le\theta\le 3\pi/2$, $r=r_\infty$) are: $u=v=0$, $w=1$, $p=0$, $T=1$, $Y_f=0$, $\rho_g=1$, while for the outflow (imposed downstream at $\xi=N_1$, $1\le\eta<N_{2\,mid}$, i.e. at $-\pi/2\le\theta\le\pi/2$, $r=r_\infty$) these conditions are: $\frac{\partial u}{\partial\xi}=\frac{\partial v}{\partial\xi}=\frac{\partial w}{\partial\xi}=\frac{\partial T}{\partial\xi}=\frac{\partial Y_f}{\partial\xi}=\frac{\partial\rho_g}{\partial\xi}=0$; $p=0$. u, v, w are flow velocity components (non-dimensionalized by U'_∞) in (x, y, z) cartesian coordinates.

2.5. Symmetry conditions

Since the cylindrical vortex tube advects with its axis of symmetry parallel to the y-axis, symmetry is maintained such that one may solve for half the spherical domain rather than the entire domain, and thus reduce the computational time. In the gas phase, these conditions are at $\zeta=1, N_3$ (i.e. at $r_i\le r\le r_\infty$, $\phi=0, \pi$)

$$\frac{\partial u}{\partial\zeta}=\frac{\partial w}{\partial\zeta}=\frac{\partial p}{\partial\zeta}=\frac{\partial T}{\partial\zeta}=\frac{\partial\rho_g}{\partial\zeta}=\frac{\partial Y_f}{\partial\zeta}=0;\quad v=0$$

In the liquid phase at $\zeta=1, N_3$ (i.e. at $0\le r\le r_i$, $\phi=0, \pi$) these conditions are

$$\frac{\partial u}{\partial\zeta}=\frac{\partial w}{\partial\zeta}=\frac{\partial p}{\partial\zeta}=\frac{\partial T}{\partial\zeta}=0;\quad v=0$$

2.6. Initial conditions and the vortex tube features

In the gas phase, the initial conditions for the velocity field are: $u_0(x, y, z) = 0$; $v_0(x, y, z) = 0$; $w_0(x, y, z) = 1$; i.e. the initial velocity in the gas phase is due to a uniform base flow. Initial conditions for the other gas properties are: $P = 0$; $T = 1$; $Y_f = 0$; $\rho_g = 1$.

At the interface, it is initially specified that: $u = 0$; $v = 0$; $w = 0$; $P = 0$; $T = T_{l,0}$; $Y_f = 0$. The imposed initial conditions inside the liquid droplet are a quiescent liquid phase and a uniform temperature distribution, T_l, $0 < T_g$, ∞. Clearly, the initial conditions have discontinuities at the gas–liquid interface but they quickly disappear after $t = 0$.

Droplet vaporization rate increases more slowly than the droplet heating rate does; therefore, the effect of vortex advection on the droplet mass transport rates becomes most significant after both the thermal and species boundary layers are established. As suggested by numerical results as well as by a comparison of relevant time-scales (Chiang, 1990; Chiang et al., 1992), the droplet is exposed to the hot gas for 300 residence time units before it is exposed to the vortex in order for the vaporization to be established; i.e. the initial condition for the vortex influence is not at $t = 0$ but at $t = 300$ (residence) time units. The initial transients caused by the injection of the droplet into the moving stream disappear by 300 time units. The temporal variables presented and discussed later as well have the time $t = 300^+$.

The vortex is introduced upstream of the droplet, advects with the superimposed uniform flow, and is an initially cylindrical tube whose axis of symmetry is initially normal to the uniform flow and parallel to the y-axis. The initially two-dimensional Rankine vortex tube (Saffman, 1992) has a small central core; within this core, the initial velocity distribution in the vortex tube is that of solid body rotation reaching an imposed maximum tangential velocity (normalized by U'_∞) denoted by v_{max} at a specified radius σ (normalized by a'). Outside this inner core, the vortex induces a velocity field of a potential vortex that vanishes as $r \to \infty$. Therefore, to introduce the vortex, at $t = 300$ the following values are added to the u and w components of gas velocity

$$u_0(x, y, z) = \frac{\Gamma_0}{\pi} \frac{z - z_{v0}}{\left[(x - x_{v0})^2 + (z - z_{v0})^2 + \sigma_0^2\right]}$$

$$w_0(x, y, z) = \frac{\Gamma_0}{\pi} \frac{x - x_{v0}}{\left[(x - x_{v0})^2 + (z - z_{v0})^2 + \sigma_0^2\right]}$$

where Γ_0 is the initial non-dimensional vortex circulation at radius σ_0. Γ_0 is positive for counterclockwise vortex rotation, and x_{v0} and z_{v0} denote the initial location of the vortex tube center. The initial vortex tube circulation is $\Gamma_0 = 2\pi\sigma_0 v_{max\,0}$. After this initial introduction of the vortex, the advection, diffusion, and distortion (strain) on the vortex is determined through the solution of the Navier–Stokes equations.

2.7. Thermophysical properties

Unlike the two previous studies (Masoudi and Sirignano, 1997, 1998) where the thermophysical properties in the gas phase were assumed invariant to the temperature, here

these properties are temperature and composition dependent; specifically, the density $\rho = \rho(T, P, Y_f, \ldots)$. Since momentum and kinetic energy fluxes (per unit volume) are $\sim \rho u^2$ and $\sim \rho u^3$, respectively, they locally depend on the temperature and the composition, as well. Near the droplet, where the temperature and concentration fields have their largest gradients, the underlying transport mechanisms and the corresponding boundary layers (momentum, temperature, species) are influenced by the thermophysical properties variations.

In addition to the density, viscosity, thermal conductivity, and heat capacity, the binary diffusion coefficient of the air–fuel vapor mixture and the latent heat of vaporization are computed following Abramzon and Sirignano (1987, 1989). Liquid heat capacity and viscosity are computed using the methods of Rowlinson and Orrick-Erbar, respectively, recommended by Reid et al. (1987). These thermophysical properties have been widely used in vaporizing droplet computations (Abramzon and Sirignano, 1987; Chiang, 1990; Chiang et al., 1992; Shih and Megaridis, 1996). To compute the thermocapillary forces in interface conditions, surface tension values were borrowed from the table values of Vargaftik (1975) and included per recommendations of Niazmand et al. (1994) and Shih and Megaridis (1996).

2.8. Numerical solution

These equations and their initial, boundary and interface conditions are nonlinear, coupled, and complicated enough to eliminate the possibility of an analytical solution and to require a computational approach.

The numerical procedure employed here is similar to the previous methods (Kim et al., 1993, 1995, 1997; Masoudi and Sirignano, 1997, 1998), i.e the equations are solved sequentially and the set of equations are iterated until convergence is achieved. The mass conservation equation is indirectly satisfied by the pressure correction equation, an elliptic equation suited to a solution by the successive-over-relaxation (SOR) method. However, the momentum, temperature, and species equations are parabolic and so are solved by an alternate direction predictor–corrector (ADPC) method.

Since, the thermophysical properties vary due to temperature and composition, the properties are computed at each node according to the local temperature and fuel mass fraction. The droplet size is also accordingly adjusted at each time-step with its new size resulting from the droplet mass vaporization. Since the droplet radius reduces due to its vaporization, the grid locations are adjusted at each time step to accommodate the droplet surface regression.

The drag coefficient and the Nusselt and Sherwood numbers are calculated iteratively using a convergence criterion at each time step. More details of the computational procedure have been previously reported (Kim et al., 1993, 1995, 1997).

2.9. Droplet convective heat and mass transfer

The droplet convective heat transfer, represented by its Nusselt number, is computed through $Nu(t) = 2a'h'/k'_g$ (with h' being the dimensional convective heat transfer coefficient) which after a standard simplification and non-dimensionalization yields

$$Nu(t) = \frac{a\int_0^{\pi}\int_0^{\pi} \kappa_g \frac{\partial T_g}{\partial r}(t)\Big|_s \sin\theta \, d\theta \, d\phi}{\pi\left[1 - T_{s,\,av}(t)\right]} \tag{9}$$

where $T_{s,\,av}$ is the droplet surface temperature averaged over its surface area.

Likewise, the droplet vaporization due to the forced convection of the hot gas is commonly portrayed using $Sh(t) = 2a'h'_m/D'_g$ (with h'_m being the dimensional convective mass transfer coefficient) which after a standard simplification and non-dimensionalization yields

$$Sh(t) = \frac{a\int_0^{\pi}\int_0^{\pi} \rho_g D_g \frac{\partial Y_f}{\partial r}(t)\Big|_s \sin\theta \, d\theta \, d\phi}{\pi\left[Y_{f,\,\infty} - Y_{f_{s,\,av}}(t)\right]} \tag{10}$$

where $Y_{f_{s,\,av}}$ is the fuel mass fraction at the droplet surface averaged over its surface area.

In the absence of an advecting vortex, the flow is axisymmetric; however, the vortex advection breaks down the flow axisymmetry, the Nusselt and Sherwood numbers vary continually and do not attain steady values. Practically, therefore, it is more convenient to obtain overall estimates by considering their time-averaged and root-mean-squared values according to

$$\bar{\phi} = \frac{1}{t_2 - t_1}\int_{t1}^{t2} \phi(t) \, dt \tag{11}$$

and

$$\phi_{rms} = \sqrt{\overline{\left[\phi(t) - \bar{\phi}\right]^2}} = \sqrt{\frac{1}{t_2 - t_1}\int_{t1}^{t2}\left[\phi(t) - \bar{\phi}\right]^2 dt}. \tag{12}$$

where $\phi(t)$ and $\bar{\phi}$ are the temporal and time-averaged Nusselt or Sherwood number, $Nu(t)$ and $\overline{Nu}$, or $Sh(t)$ and $\overline{Sh}$, respectively.

3. Results

In this section, the relevant temporal variables are quantified and qualitative observations of the vortex effect on the global droplet transport mechanisms are made. Finally, correlations describing global self-similarity in the observed behavior are obtained and discussed.

3.1. Vortex motion influencing the global flow field

Fig. 2(a1, b1) show the axisymmetric gas temperature and species fields (i.e. without vortex advection). Fig. 2(a2, b2) are the same fields, respectively, influenced by vortex advection. (All figures in this section depict the events in the (x, z) plane of flow symmetry where maximum interaction between the vortex and the droplet is observed.) The influence of the vortex advection on the said transport mechanisms is apparent. Recall that vortex advection does not

only break down the flow symmetry, it could also drastically change the structure of the recirculation zone in the droplet near wake (Kim et al., 1995). A localized pressure drop due to the augmented velocity field near the vortex location induces a deflection in the velocity boundary layer toward the vortex. Since Prandtl and Schmidt numbers are $Pr \sim 1$ and $Sc \sim 3$ (n-octane), the three boundary layers have modestly differing lengths; hence, this deflection in the velocity boundary layer is repeated in a qualitatively similar way in the thermal and species boundary layers as well. This natural consequence of the coupling between the velocity and the latter two boundary layers underlines the powerful roles of the convective terms in the

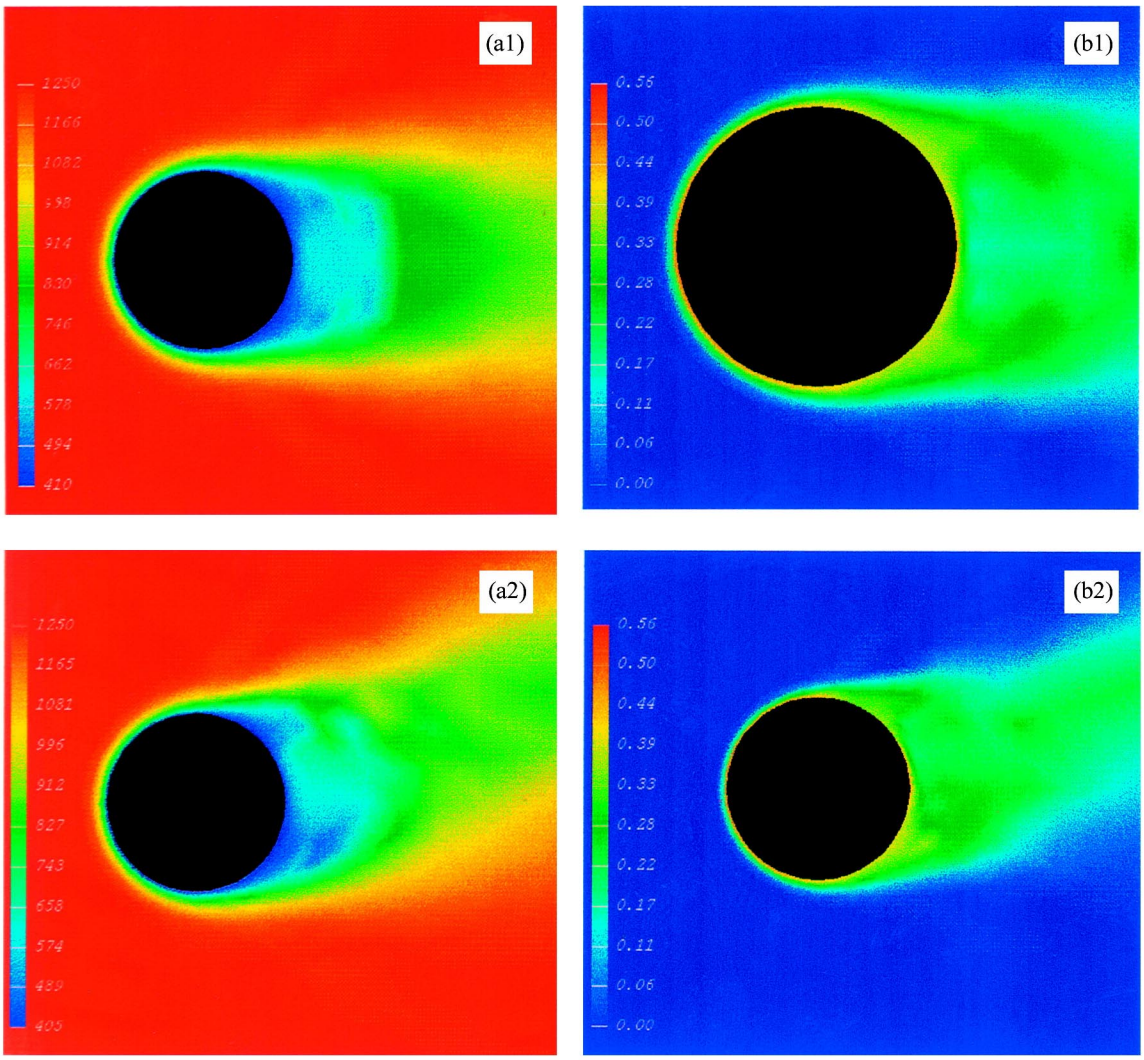

Fig. 2. (a1) Temperature, and (b1) species fields of the droplet in an axisymmetric flow; (a2) temperature, and (b2) species fields of the droplet in the presence of vortex advection ($d_0 = 2$, $\sigma_0 = 2$, $v_{\max,\,0} = 0.3$, $Re = 100$, $t = 312$).

governing equations of all three transport mechanisms in this study. More information on the distortion of the droplet velocity boundary layer and also the variations in its pressure field due to the vortex have been reported by Kim et al. (1995) and Masoudi (1998).

In this variable property simulation, gas density strongly depends on the local temperature and, therefore, inside the thermal boundary layer where $T_g < T_{g,\infty}$, density values are larger than the free stream values. This density gradient effect (in the presence of pressure gradients) results in nonuniform acceleration and strain. The strain modifies length scales, thereby modifying diffusion rates. Otherwise stated, density variation has an augmenting effect on the heating and vaporization rates when the vortex advects through boundary layers.

The vortex effects are, however, not as pronounced in the droplet interior as they are in the gas phase (Masoudi, 1998). The large density and viscosity ratios between the liquid and the gas phase (or, equivalently, the large kinematic viscosity ratio $\nu_l'/\nu_g' = 25$) inhibit the influence of the flow fluctuations in the outer stream on the internal droplet developments. Only fluctuations with long time periods can be expected to have significant effects on the microstructure of the liquid phase.

3.2. Vortex motion influencing droplet surface properties

Fig. 3(a, b) show the effect of vortex advection on the vaporizing droplet Nusselt number for different values of the vortex initial location d_0. (The droplet has lapsed 300 residence time units before exposure to vortex motion.) The maximum variation in $Nu(t)$ (at $d_0 = 2$) is 2–3.5%. Comparison with the nearly 10% variation observed in the simulation of a non-vaporizing droplet (Masoudi and Sirignano, 1997) shows that the droplet heating and its variations due to vortex advection are reduced due to droplet vaporization forming a layer of fuel vapor near the droplet surface. The effects on mass transport and Sherwood number will be shown to be much greater.

The circulation of the initially Rankine vortex is $\Gamma_0 = 2\pi\sigma_0 v_{\max,0}$ and, therefore, depends on both its maximum initial tangential velocity ($v_{\max,0}$) and its initial size (σ_0). The Nusselt number and Sherwood number do not correlate with only the circulation. Rather, they correlate with different powers of vortex maximum tangential velocity and size. Fig. 4(a, b) indicate a maximum variation of about 2–3% on $Nu(t)$ within the range of the parameters. (In the earlier constant property non-vaporizing droplet simulation by Masoudi and Sirignano (1997), these effects were nearly twice as large.) The heating rate of a vaporizing droplet with convective heating shows little sensitivity to vortex-induced perturbations. This is due to the inhibiting effect of the vaporized fuel vapor near the droplet surface: this layer 'cuts off' the droplet surface heating from the 'events' in the outer stream. This observation is in agreement with the published information on the attenuating effect of the fuel vapor layer on droplet surface heating in axisymmetric flows without advecting vortices (Renksizbulut and Yuen, 1983; Haywood et al., 1989; Chiang, 1990; Chiang et al., 1992; Niazmand et al., 1994; Shih and Megaridis, 1996). This 'buffer layer' is non-existing for a nonvaporizing droplet or for a solid sphere.

Fig. 5(a, b) show the effect of vortex advection on the vaporizing droplet Sherwood number for different values of the vortex initial location d_0. Fig. 5(b) shows that the maximum variation in the droplet temporal Sherwood number takes place at $d_0 = 2$, is nearly 12%, and

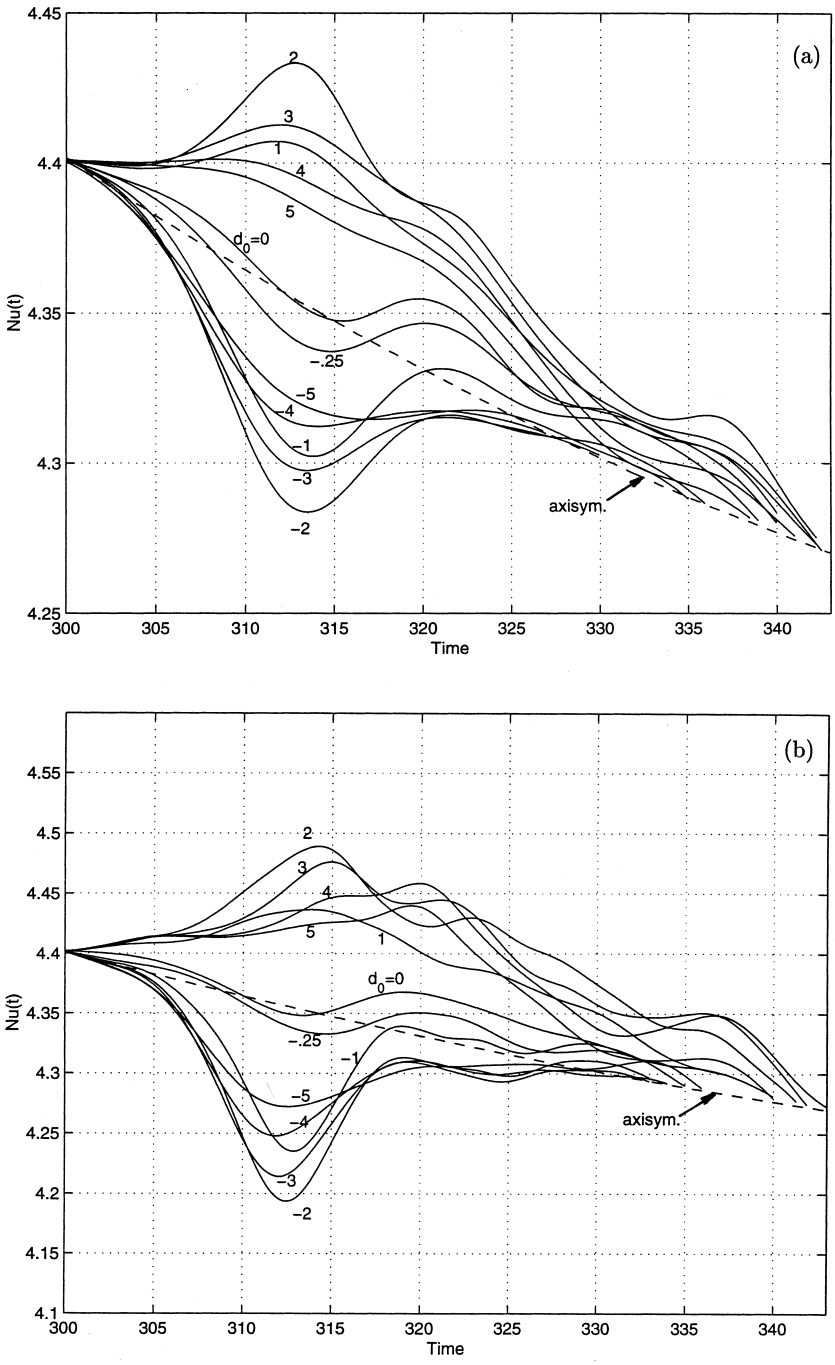

Fig. 3. Influence of the vortex initial offset distance d_0 on the droplet Nusselt number: (a) vortex advecting with d_0 in $-5 \le d_0 \le 5$, ($Re = 100$, $\sigma_0 = 1$, $v_{\max,\,0} = 0.2$); (b) same, $v_{\max,\,0} = 0.4$.

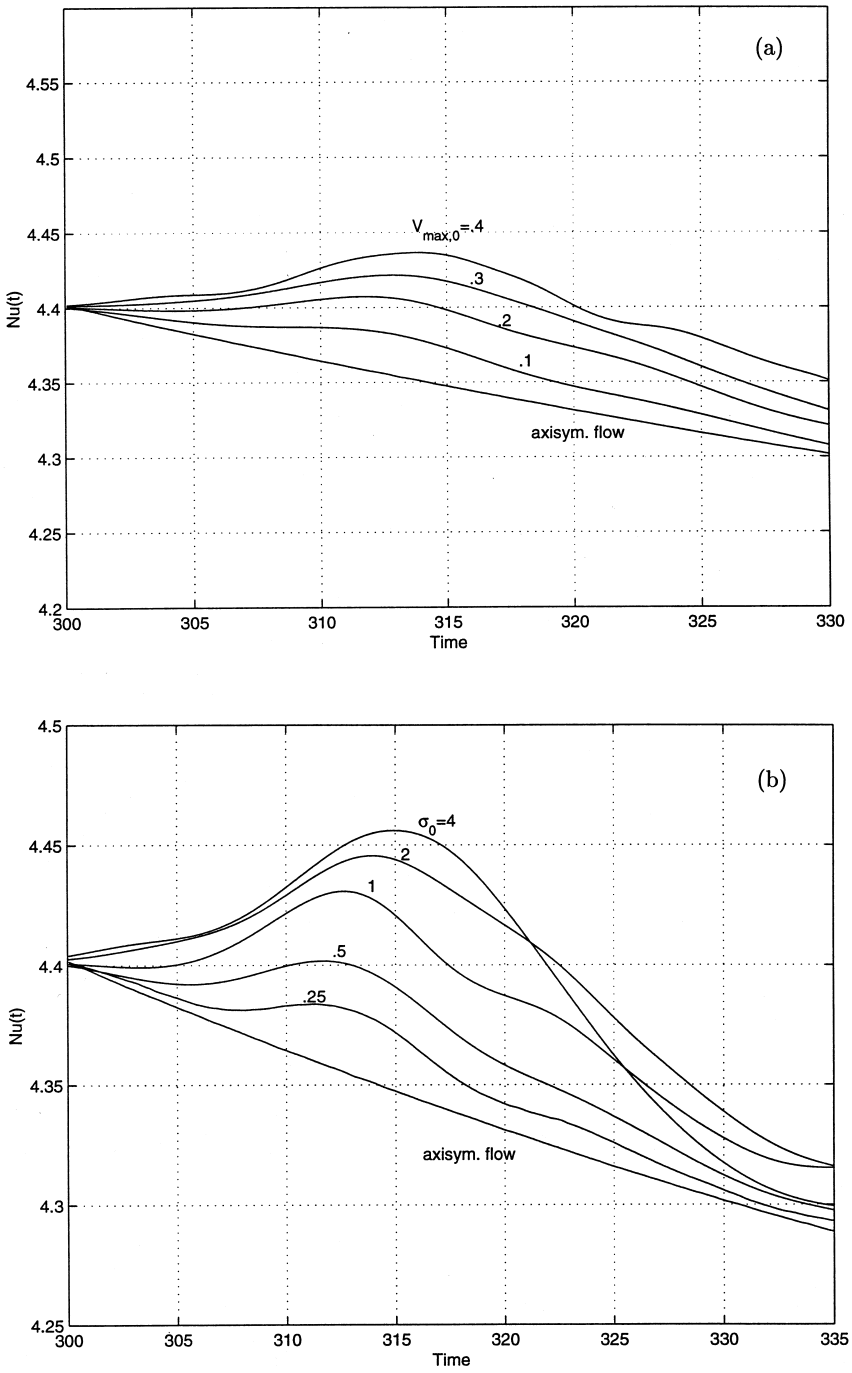

Fig. 4. Influence of the vortex (a) initial strength $v_{max,\,0}$ and (b) initial size σ_0 on the Nusselt number ((a): $Re = 100$, $d_0 = 1$, $\sigma_0 = 1$; (b): $Re = 100$, $d_0 = 2$, $v_{max,\,0} = 0.2$).

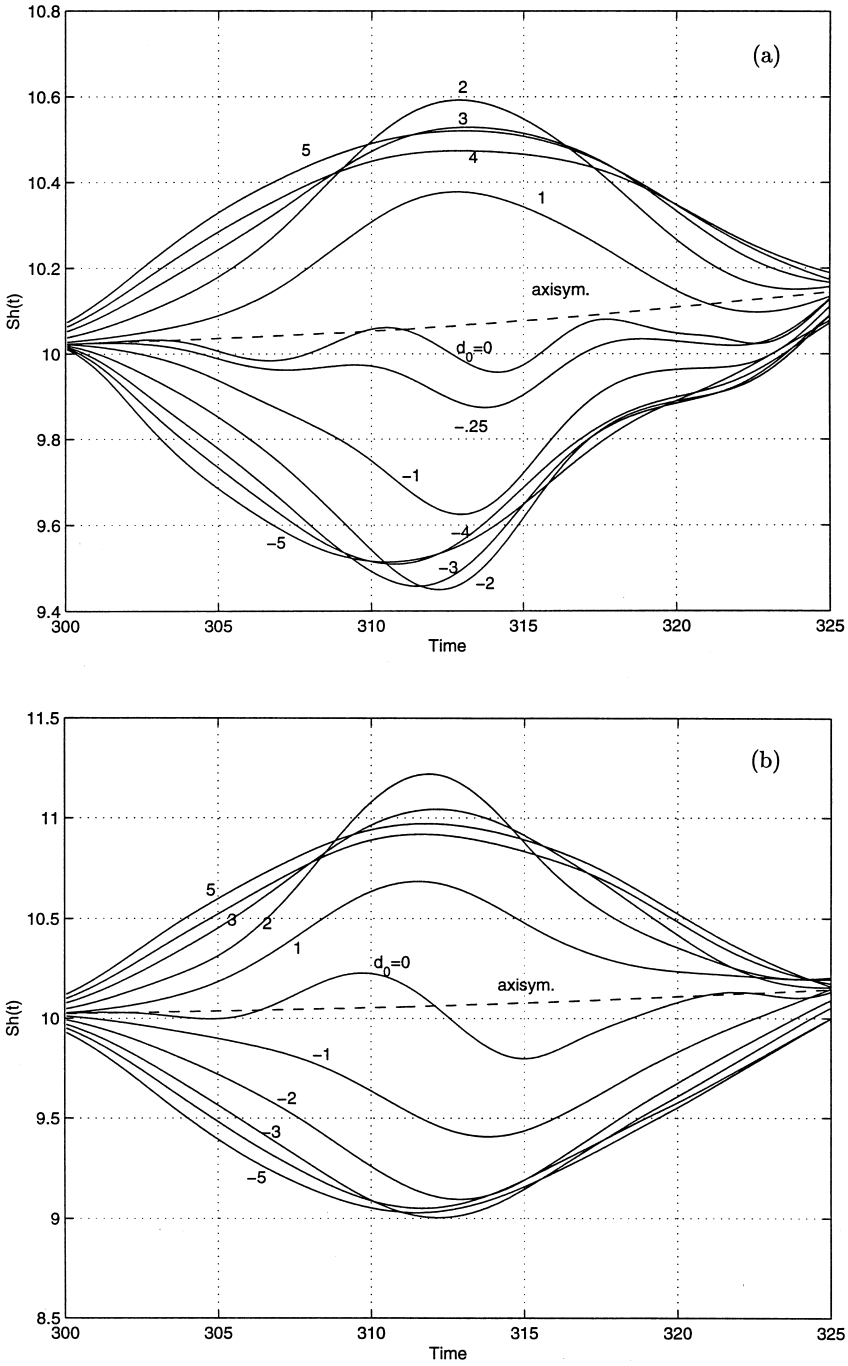

Fig. 5. Influence of the vortex initial offset distance d_0 on the Sherwood number (a) vortex advecting with d_0 in $-5 \leq d_0 \leq 5$, ($Re = 100$, $\sigma_0 = 1$, $v_{\max,\,0} = 0.2$); (b) same, $v_{\max,\,0} = 0.4$.

is, therefore, about five-fold larger than the maximum variations in the temporal Nusselt number (Fig. 3(b)) due to the same vortex. Fig. 6(a, b) demonstrate the sensitivity of the droplet Sherwood number and the vaporization rate to the vortex maximum tangential velocity and size, respectively; the vortex-induced variations are about 6–8%. These observations are quantified, correlated, and further discussed in the following sections.

3.3. Global self-similarity

In the absence of the vortex, Nu and Sh are same as those in an axisymmetric system; i.e. they are identical with Nu_{ax} and Sh_{ax}, so that one may approximate the droplet Nusselt or Sherwood number using the correlations from Renksizbulut and Yuen (1983) or Abramzon and Sirignano (1987, 1989), for instance. With the vortex present in the domain, however, the axisymmetric flow correlations for Nu and Sh lose their applicability and new correlations accounting for the effect of the advecting vortex are to be sought.

The influence of vortex motion on the heating of a non-vaporizing droplet, such as for vortex–droplet collision taking place in the beginning of the droplet injection into the combustion chamber, could be predicted using the self-similar correlation (Masoudi and Sirignano, 1997)

$$\frac{\overline{Nu}}{\overline{Nu}_{ax}} = 1 + 0.019\frac{\Gamma_0}{2\pi}Re^{0.40}\tanh\left(0.50\frac{d_0}{\sigma_0^{0.6}}\right) \tag{13}$$

(with Reynolds number defined based on the droplet diameter, $Re = U'_\infty 2a'_0/\nu'_\infty$).

With vaporization present, the problem is complicated due to the Stefan flux near the droplet free surface. New correlations are, therefore, needed for a vaporizing droplet Nusselt number influenced by vortex motion.

Fig. 3(a, b) show that when the counterclockwise vortex initial location upstream of the droplet is 'above' the base flow symmetry axis in the $(x–z)$ plane of symmetry ($d_0 > 0$), the droplet Nusselt number, while fluctuating due to vortex motion, is continuously above the axisymmetric Nusselt number; therefore, such a vortex with a positive offset distance has an augmenting effect on the droplet Nusselt number. Likewise, a vortex with a negative offset distance attenuates the droplet Nusselt number. The maximum deviation, i.e. $|Nu(t)/Nu_{ax}(t) - 1|_{max}$ happens when the vortex advects closest to the droplet, usually about 12 residence time units after its introduction.

However, with the Stefan flux present, the temporal variations in Nusselt number due to the advecting vortex are usually small. The same is true for $\overline{Nu}/\overline{Nu}_{ax}$. This relatively weak consequence of the vortex advection on the droplet heating should have little practical consequence. Therefore, we do not pursue and correlate for the Nusselt number in this vaporizing case. Rather, we emphasize the Sherwood number correlation.

The influence of the vortex advection on the droplet Sherwood number, shown in Fig. 5(a, b), is qualitatively similar to that for the droplet Nusselt number (Fig. 3(a, b)); i.e. a vortex with a counterclockwise circulation advecting above/below the non-fluctuating base flow symmetry axis continuously augments/attenuates the droplet Sherwood number. The similarity

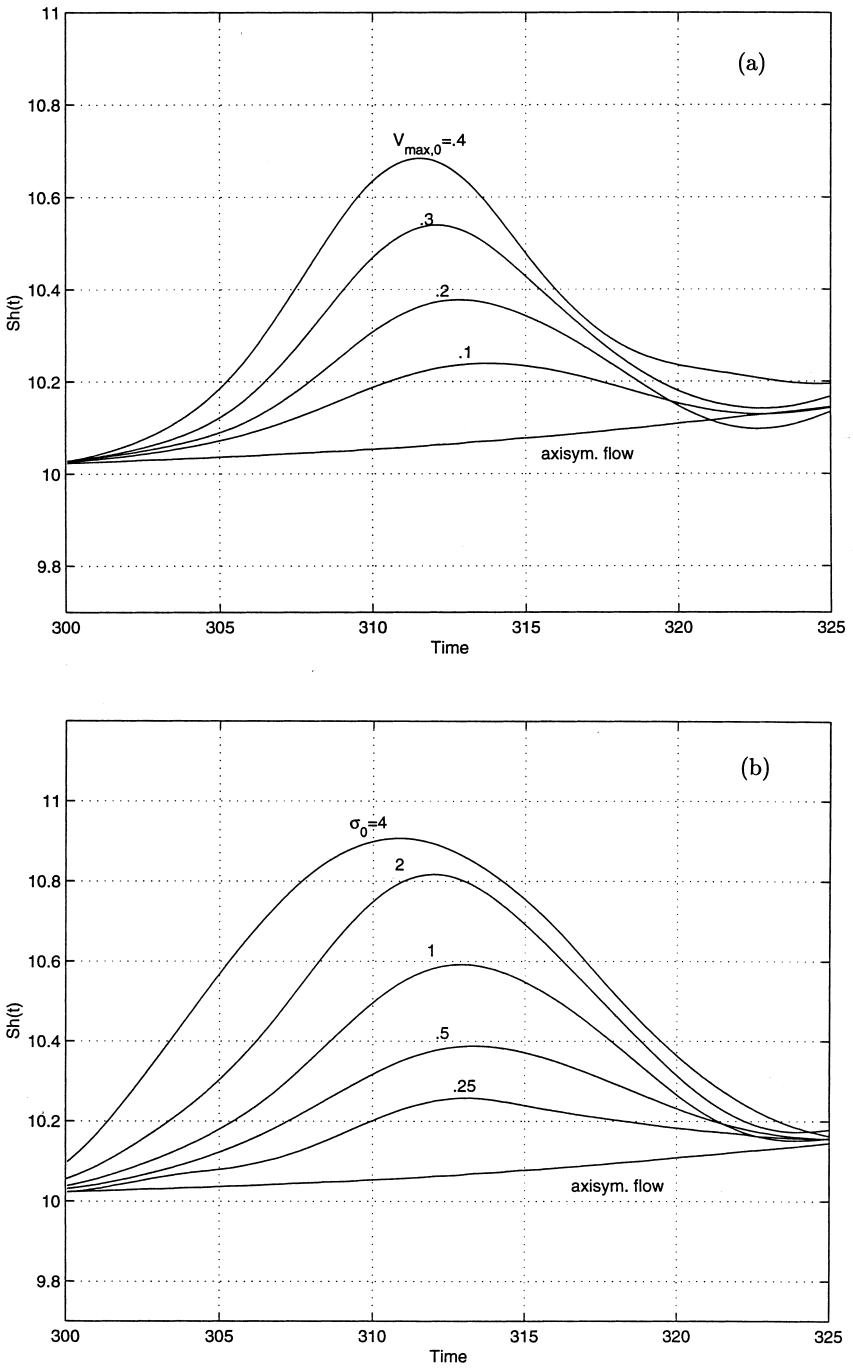

Fig. 6. Influence of the vortex (a) initial strength $v_{\max,0}$ and (b) initial size σ_0 on the Sherwood number; ((a): $Re = 100$, $d_0 = 1$, $\sigma_0 = 1$; (b): $Re = 100$, $d_0 = 2$, $v_{\max,0} = 0.2$).

is explained by the similarity between energy and species equations and their identical dependence on the velocity field and, therefore, on the vortex advection.

Quantitatively, the variations in the droplet temporal Sherwood number due to the vortex are, however, more significant than temporal variations in Nusselt number. Further, the fluctuations induced by the vortex expectedly increase with an increase in vortex size, strength, or flow Reynolds number. Therefore, one should regard $|Sh(t)/Sh_{ax}(t)|_{max}$ as a measure of the perturbations in Sherwood number. It is found that the measured Sherwood number variations collapse into a single functional form,

$$\left[\frac{Sh(t)}{Sh_{ax}(t)}\right]_{max} = 1 + 0.013\left(\frac{\Gamma_0}{2\pi}\right)^{0.85} Re^{0.75} \tanh\left(0.75\frac{d_0}{\sigma_0^{0.80}}\right) \tag{14}$$

within $10 \le Re = U'_\infty a'_0/\nu'_\infty \le 50$; $0.25 \le \sigma_0 \le 4$; $0.1 \le v_{max,\,0} \le 0.4$; $-5 \le d_0 \le 5$. This covers a range of vortex circulation varying by nearly two order-of-magnitudes: $\Gamma_0 \in (0.16, 10.05)$, see Fig. 7. The correlation coefficient for the above fit is $r_1 = 0.910$; $(r \equiv 1 - [\sum_{i=1}^{n}(y_{actual_i}/y_{fit_i} - 1)^2]^{0.5}$; $y = [Sh(t)/Sh_{ax}(t)]_{max})$.

It is equally useful to examine time-averaged values of these perturbations, $\overline{Sh}/\overline{Sh_{ax}}$, which collapse into

$$\frac{\overline{Sh}}{\overline{Sh_{ax}}} = 1 + 0.0047\left(\frac{\Gamma_0}{2\pi}\right)^{0.78} Re^{0.80} \tanh\left(0.65\frac{d_0}{\sigma_0^{0.55}}\right) \tag{15}$$

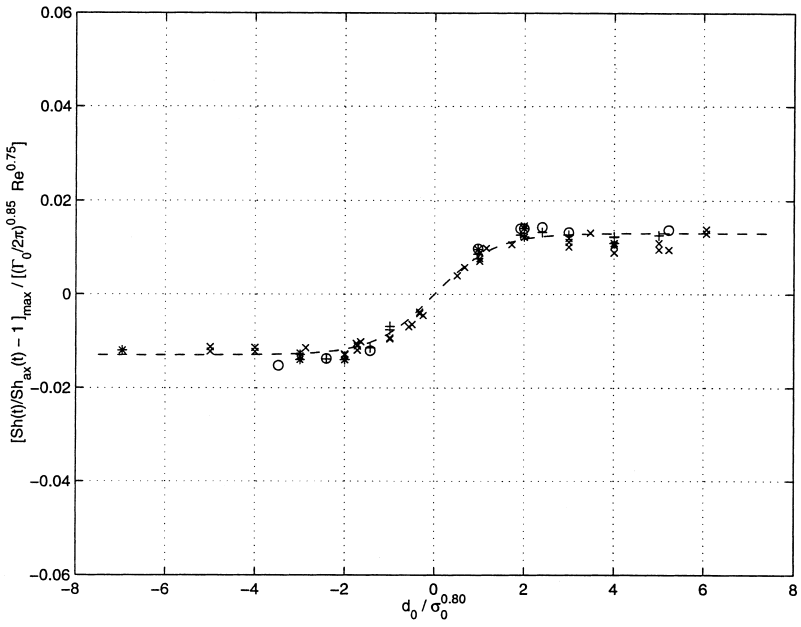

Fig. 7. Existence of global self-similarity in the temporal Sherwood number fluctuations due to vortex advection, Eq. (14).

within the same range noted above, see Fig. 8. The correlation coefficient for this fit is $r_2 = 0.963$.

These two correlations signify the existence of global self-similarity in Sherwood number deviations due to vortex advection near the droplet and quantify such fluctuations in this unsteady problem. They also complement the existing correlations for a vaporizing droplet Sherwood number in axisymmetric flows that occur in the absence of an advecting vortex (Renksizbulut and Yuen, 1983; Abramzon and Sirignano, 1987, 1989).

Eqs. (14) and (15) and their comparison with our data are shown in Figs. 7 and 8, respectively. Note that for $|d_0/\sigma_0^m| \to 5$, both $[Sh(t)/Sh_{ax}(t)]_{max}$ and $\overline{Sh}/\overline{Sh_{ax}}$ approach an asymptote; here, profiles of $Sh(t)$ are still at least modestly different, shown in Fig. 5(a, b).

According to the similarity hypothesis, in an axisymmetric flow and when thermophysical properties are constant in time and space, Nusselt and Sherwood numbers have identical dependence on the flow Reynolds number (Renksizbulut and Yuen, 1983; Abramzon and Sirignano, 1987, 1989;), this is the consequence of identical dependence of energy and species equations on the flow field. This insight could be further extended when studying perturbed flows; i.e. it is perhaps plausible if one expects that Nusselt and Sherwood numbers have similar dependence on the flow perturbations, as well, represented by the vortex circulation Γ_0. So, the two correlations (13) and (15) are similar.

One would expect the observed deviation in Nu and Sh from those in steady axisymmetric flows would go to zero as $d_0 \to \infty$. In the range of d_0 examined ($d_0 \in [-5, 5]$), such a decay is not observed so that presumably the characteristic length for this decay is larger than five non-dimensional units. Correlations (14) and (15) indicate that a change in the sign of either d_0 or

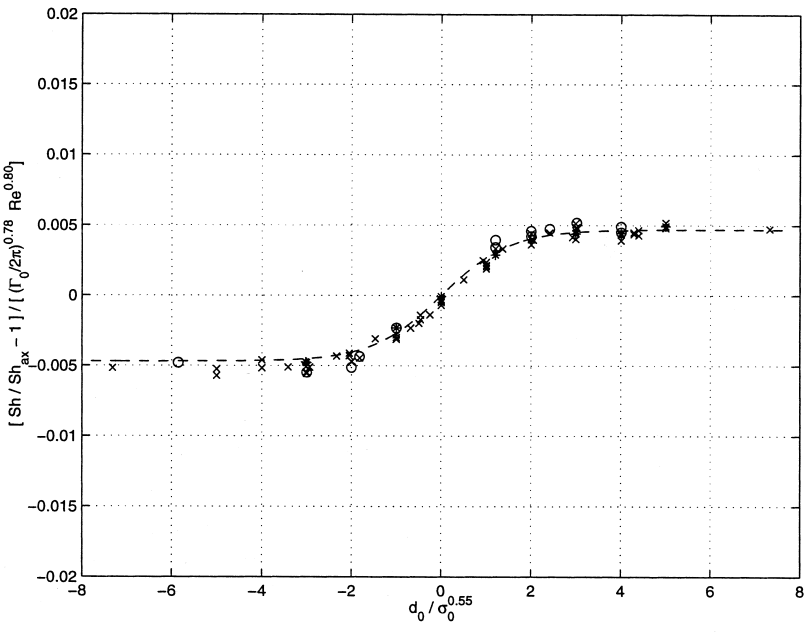

Fig. 8. Existence of global self-similarity in the time-averaged Sherwood number fluctuations due to vortex advection, Eq. (15).

circulation produces a change in the sign of the deviation of Sherwood number from the non-fluctuating base axisymmetric value. Finally, one should note that these correlations hold for bounded values of the fluctuating velocity; in particular, the vortex is not strong enough to reverse the free stream flow direction, (v'_{max}, $0/U'_{\infty} < 1$).

3.4. Other fuels: n-heptane and n-decane droplets

In this section, the goal is to compare the results for the 'base' fuel droplet *n*-octane, to other fuel droplets of higher and lower volatility, *n*-heptane and *n*-decane, respectively. See Section 2.7 for information on the computation of fuel properties and the correlations utilized and Masoudi (1998) for additional information on each fuel.

Fig. 9(a, b, c) show the thermal field for the interior of the three fuel droplets. The droplet internal temperature is higher for *n*-decane than for *n*-octane (and, likewise, higher for *n*-octane than for *n*-heptane); this is due to the difference in the heat stored inside the droplet which increases with an increase in the droplet boiling temperature.

Fig. 10(a1, b1, c1) show the external thermal boundary layers and wakes of *n*-heptane, *n*-octane, and *n*-decane, respectively. The figures indicate that the thermal boundary layer of *n*-heptane is thicker, for instance, than that of *n*-decane. This agrees with the analysis of Abramzon and Sirignano (1987) that the thermal layer thickness increases with an increase in the Spalding transfer number B.

Fig. 10(a2, b2, c2) show the species boundary layers and wakes of *n*-heptane, *n*-octane, and *n*-decane, respectively. They indicate that the droplet vaporization mostly takes place on the droplet frontal face also reported by other investigators (e.g., Renksizbulut and Yuen, 1983; Haywood et al., 1989; Chiang, 1990), this is due to the substantially thinner local boundary layer, itself the consequence of the faster convective rate on the droplet frontal area. A comparison of the three species boundary layers also shows that a heavier fuel (*n*-decane) has a shorter and also 'thicker' boundary layer. A decrease in the boundary layer length is simply a result of a decrease in vaporization, in agreement with the analysis of Abramzon and Sirignano (1987) for a decrease in B; local 'thickening' of the boundary layer is expected for the heavier fuel since the transport of a heavier fuel vapor becomes increasingly slower by the main stream flow, which is then followed by a larger accumulation of the fuel layer in the boundary layer.

Fig. 11(a, b) show the effect of the vortex advection on the temporal Nusselt and Sherwood numbers of the three fuel droplets under consideration. Values of $[Nu(t)/Nu_{ax}(t)]_{max}$ and $[Sh(t)/Sh_{ax}(t)]_{max}$ for these three different fuel droplets shows that within a negligible deviation of 1% and 2%, respectively, measured perturbations due to vortex advection remain identical for the three fuels; moreover, computing and comparing the time-averaged quantities $\overline{Nu}/\overline{Nu_{ax}}$ and $\overline{Sh}/\overline{Sh_{ax}}$ for these three different fuel droplets shows that, within 0.5% and 1%, respectively, the observed deviations due to vortex advection remain identical for all three fuel droplets. Therefore, one may use Eqs. (14) and (15) to approximately predict the influence of vortex collision on the droplet Sherwood number for any of the three fuel droplets discussed here.

The reason for this applicability of Eqs. (14) and (15), originally developed for an *n*-octane fuel droplet only, to *n*-heptane and *n*-decane is a simple one; published literature (Sirignano, 1983; Renksizbulut and Yuen, 1983; Abramzon and Sirignano, 1987, 1989; Haywood et al.,

1989) indicates that droplet heating and vaporization has a weak functional dependency on the transfer number B. Since in Eqs. (14) and (15) both the numerator and the denominator (on the left hand side) have the same dependency on B, the net ratio becomes roughly independent of B, so that the correlations hold for the other two fuels, as well. Finally, the observed weak dependence of the said results on the transfer number B suggests that Eqs. (14) and (15) could be applicable to other fuels (e.g. n-hexane and n-nonane) not considered in this study.

Previous investigation (Masoudi and Sirignano, 1997) indicates that, for a non-vaporizing

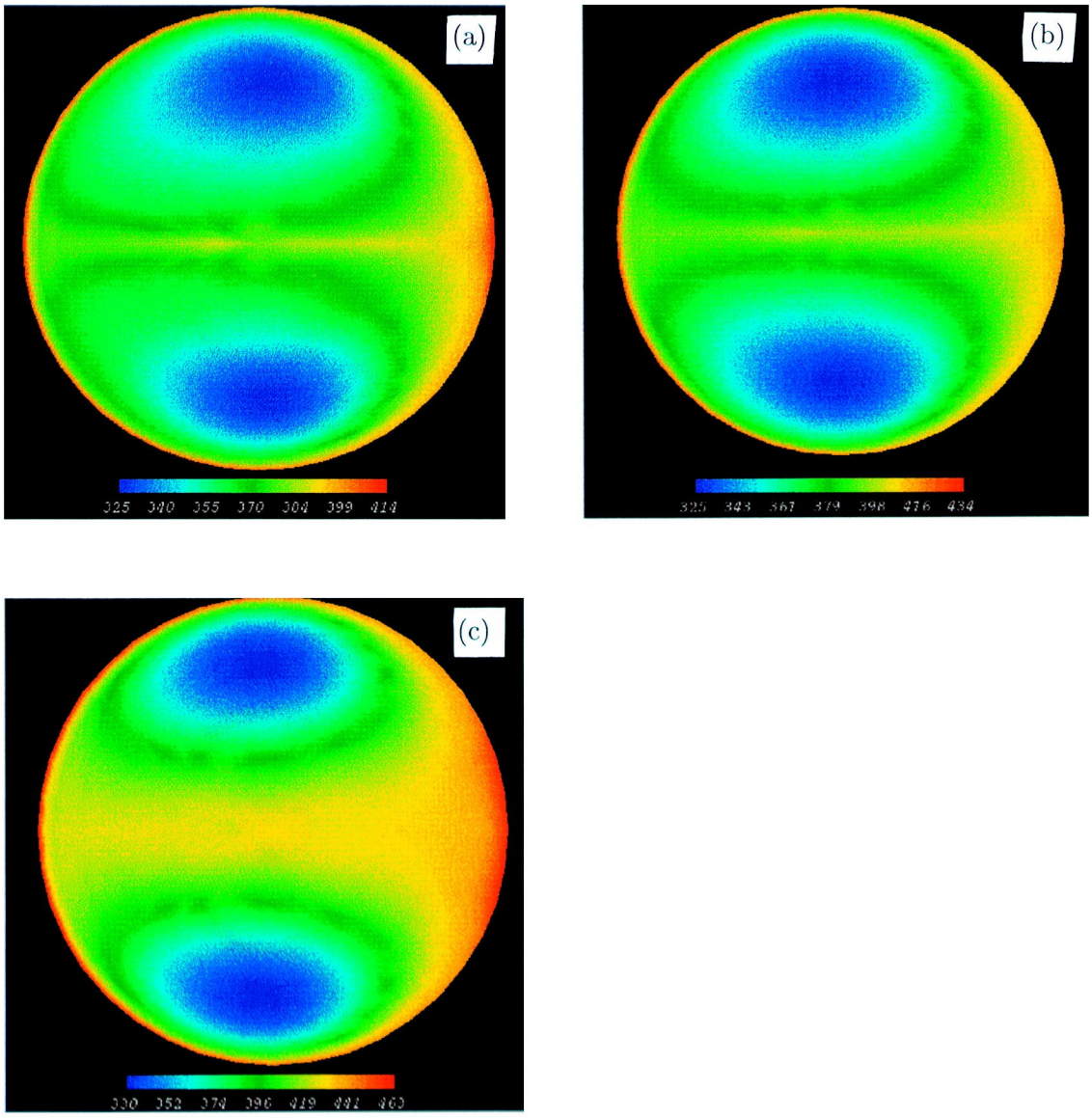

Fig. 9. Internal temperature field of the droplet for a (a) n-heptane, (b) n-octane, (c) n-decane fuel droplet ($t = 300$).

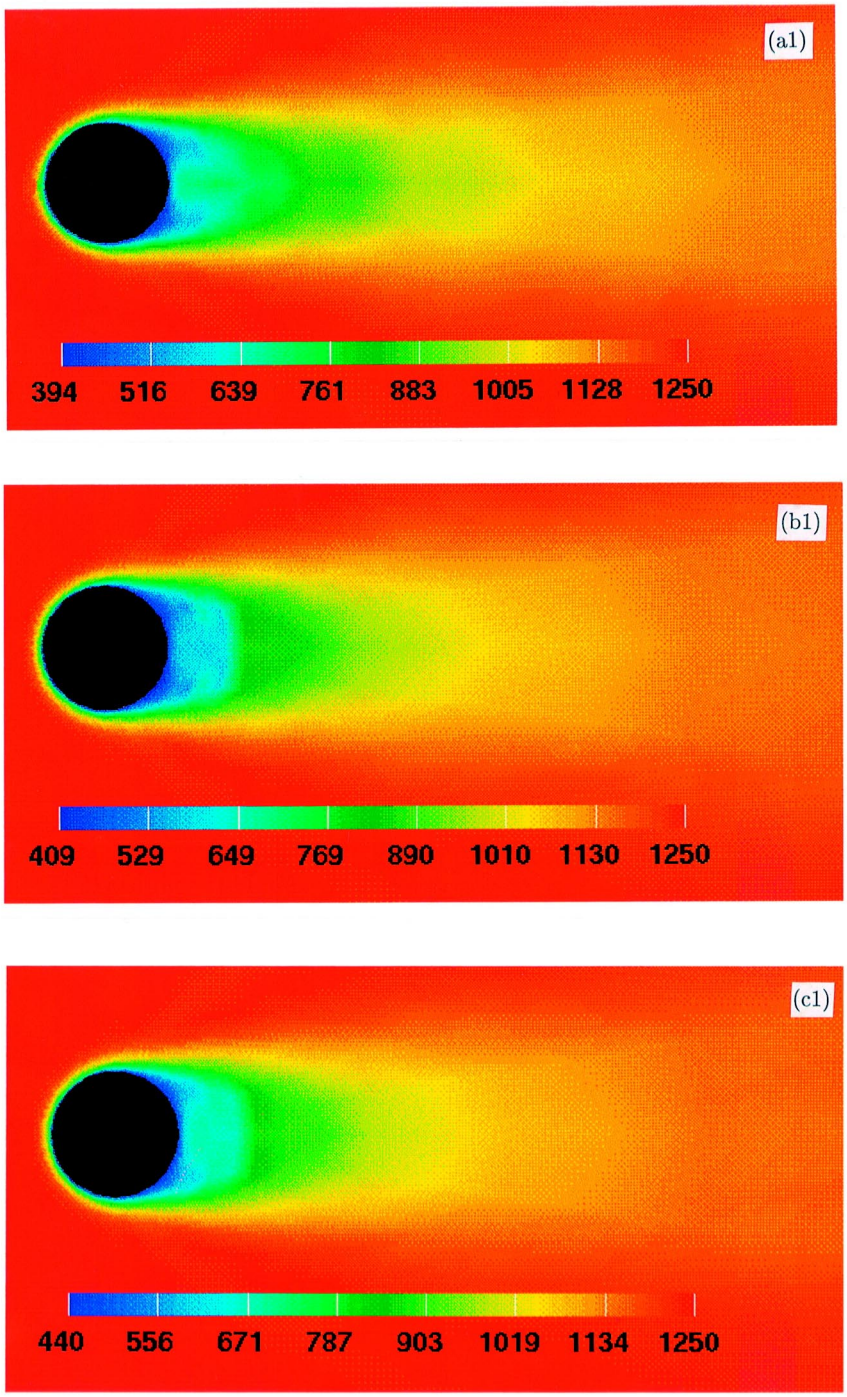

Fig. 10. External thermal boundary layer of the droplet for a (a1) *n*-heptane, (b1) *n*-octane, (c1) *n*-decane fuel droplet; species boundary layer of the droplet for a (a2) *n*-heptane, (b2) *n*-octane, (c2) *n*-decane fuel droplet (t = 300).

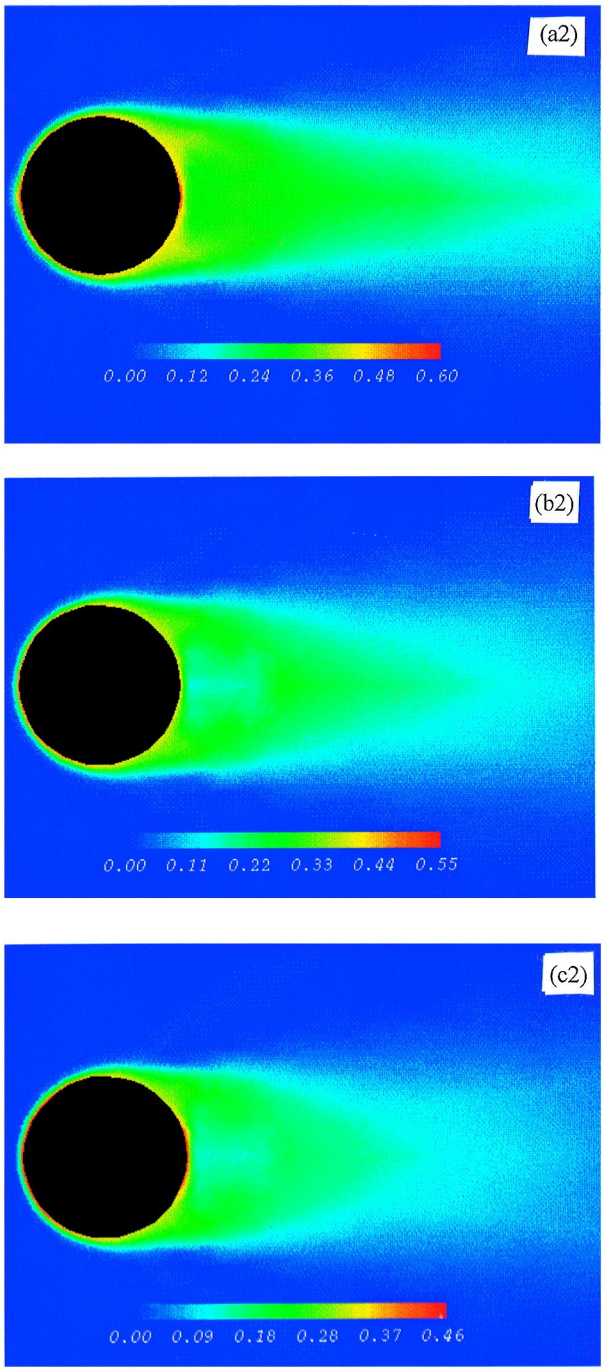

Fig. 10 (*continued*)

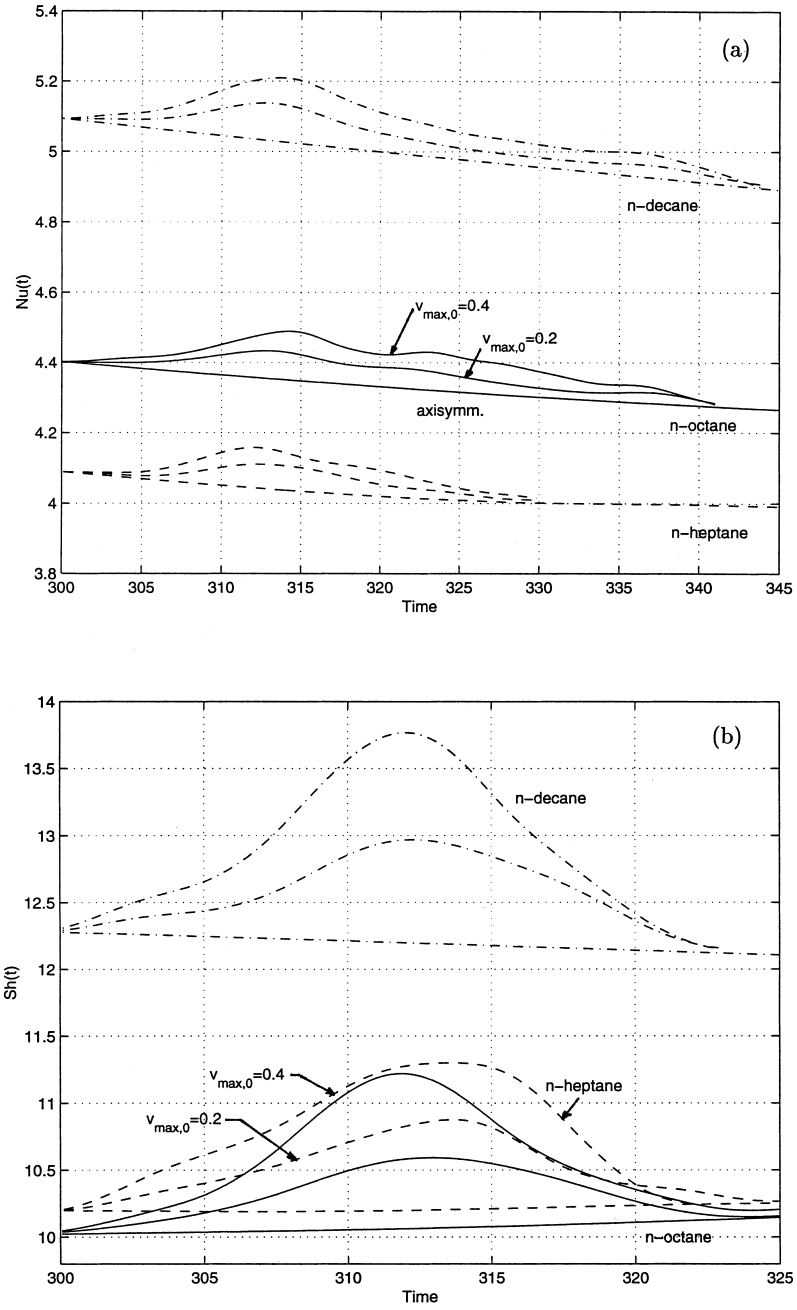

Fig. 11. Influence of the vortex advection on the (a) Nusselt number and (b) Sherwood number of *n*-heptane, *n*-octane, *n*-decane fuel droplets; ($Re = 100$, $\sigma_0 = 1$, $d_0 = 2$).

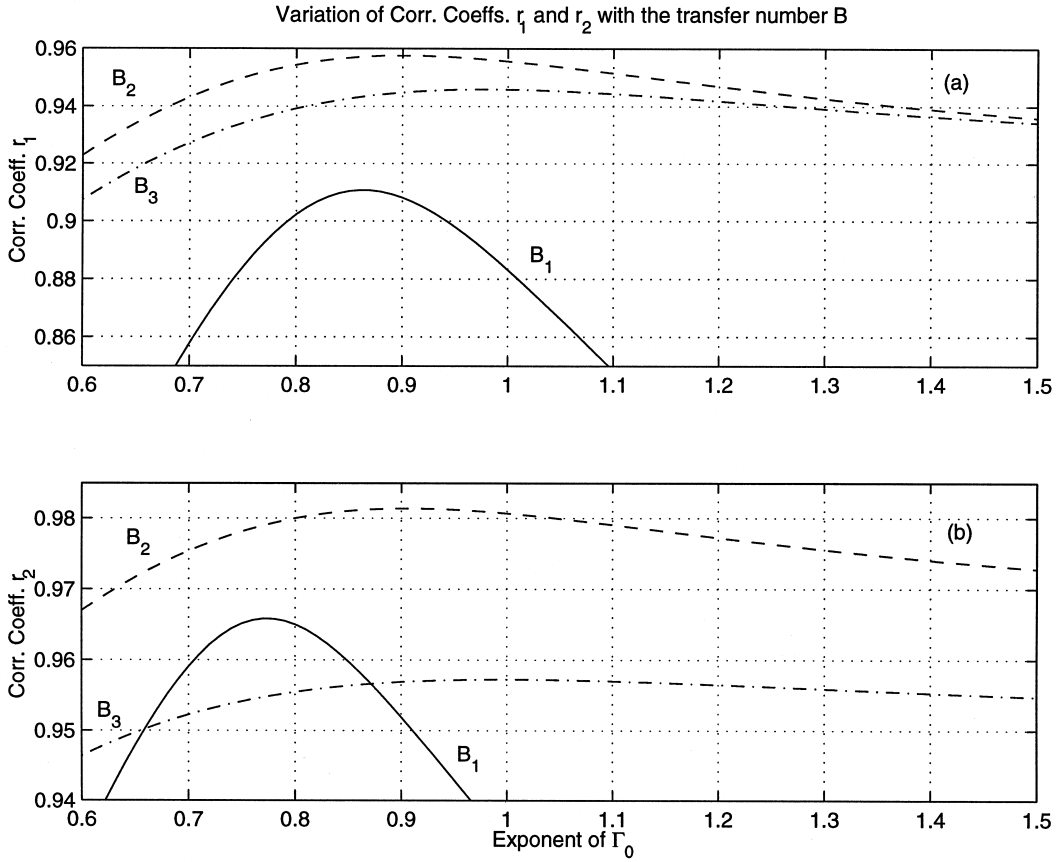

Fig. 12. Relationship between the correlation coefficients (a) r_1 (Eq. (14)) and (b) r_2 (Eq. (15)) and the exponent of vortex circulation Γ_0 for different values of the transfer number B; $B_3 < B_2 < B_1$.

droplet in a constant property domain, the net perturbation in Nusselt number varies with the vortex circulation with a unity exponent, ($Nu' \sim \Gamma_0$), and so, from similarity hypothesis, one may predict $Sh' \sim \Gamma_0$, as well. Eqs. (14) and (15) reveal that $Sh' \sim \Gamma_0^m$, $m \approx 0.8$, which closely agrees with this prediction. The slight drop in the exponent of Γ_0 from unity to 0.8 is due to the presence of the Stefan flux near the droplet inhibiting the vortex effect on the vaporization; otherwise stated, the exponent of Γ_0 depends weakly on the transfer number B; this is shown in Fig. 12; the figure indicates that as the droplet vaporization and, therefore, B is reduced (i.e. as $B \to 0$), the proper value of m appears to follow $m \to 1$, indicated by where the maximum values of the correlation coefficients r_1 and r_2 yield the best value of m for the fit.

4. Conclusions

Single droplet heating and vaporization influenced by vortex collision have been investigated. Particular attention has been paid to the transient and time-averaged values of the droplet

Nusselt and Sherwood numbers as compared to values in axisymmetric flows. Though temporal patterns of Nusselt number for a vaporizing droplet resemble those for a non-vaporizing droplet (Masoudi and Sirignano, 1997), it is observed, quantitatively, that the average variations, remain small (4% or less) within the range of the parameter study. Analogous to axisymmetric flows, where the Stefan flux reduces the droplet convective heating by forming a layer of fuel vapor near its free surface, here the Stefan flux further 'blocks' the effect of the vortical perturbations on the droplet interface as well, inhibiting Nusselt number perturbations.

Temporal patterns of Sherwood number, however, appear to be more significant quantitatively. Correlations quantifying temporal and time-averaged values of the droplet Sherwood number influenced by vortex collision vary monotonically with vortex circulation, non-fluctuating base flow Reynolds number, and exponentially with the vortex initial location. The perturbations are maximum when the Rankine vortex is initially two length-scales from the non-fluctuating base flow symmetry axis upstream of the droplet.

Though for a non-vaporizing droplet $Nu' \sim \Gamma_0$ and, therefore, according to the similarity hypothesis, one should expect $Sh' \sim \Gamma_0$, the simulations reveal that, instead, $Sh' \sim \Gamma_0^{0.78}$; the reduction in the exponent of the vortex circulation is due to the Stefan flux near the droplet reducing the flow perturbation effect on the surface vaporization and, therefore, on the Sherwood number fluctuations. Variations in the droplet Nusselt number due to the flow perturbations are similarly attenuated by the Stefan flux.

The self-similar correlations reported here are shown to be valid for at least three common fuel droplets (*n*-heptane, *n*-octane, and *n*-decane) and are expected to cover yet a larger variety of monocomponent fuels not considered in this study. These correlations complement the existing ones for droplet vaporization in axisymmetric flows that occur in the absence of an advecting vortex (Renksizbulut and Yuen, 1983; Abramzon and Sirignano, 1987, 1989). Since the effects of blended liquids or of neighboring droplets have not been considered, these correlations should not blindly be applied to multicomponent droplets or to dense sprays. However, they might still provide useful information about trends for dense sprays or for multicomponent droplet vaporization.

Some obvious and potentially interesting extensions of this work exist. Masoudi and Sirignano (1998) have demonstrated that for a non-vaporizing droplet significant augmentation in heating rate can occur due to the combination of the vortex collision and a stratified ambient temperature field near the droplet. The study of a vaporizing droplet in a gas field stratified in both vapor concentration and temperature should occur. Extensions to dense sprays, multicomponent liquids and/or near critical thermodynamic conditions would be useful. See Sirignano (1999) for discussion of those topics.

References

Abramzon, B., Sirignano, W.A., 1987. Approximate theory of a single droplet vaporization in a convective field: effects of variable properties, Stefan flow and transient liquid heating. In: ASME/JSME Thermal Engineering Conference. vol. 1. ASME, Hawaii, 11–18.

Abramzon, B., Sirignano, W.A., 1989. Droplet vaporization model for spray combustion calculations. Int. J. Heat Mass Transfer 32 (9), 1605–1618.

Bellan, J., Harstad, K., 1991. Model for evaporation of clusters of drops embedded in jet vortices. Part I. Steady injection of identical clusters. In: Heat and Mass Transfer in Fires and Combustion Systems, vol. 17. ASME, New York, pp. 65–70 ASME Winter Annual Meeting, Atlanta, Georgia.

Chiang, C.H., 1990. Isolated and interacting vaporizing fuel droplet: field calculation with variable properties. Ph.D. Dissertation, University of California, Irvine.

Chiang, C.H., Raju, M.S., Sirignano, W.A., 1992. Numerical analysis of convecting, vaporizing fuel droplet with variable properties. Int. J. Heat Mass Transfer 35 (5), 1307–1324.

Conner, J.M., Elghobashi, S.E., 1987. Numerical solution of laminar flow past a sphere with surface mass transfer. Numerical Heat Transfer 12, 57–82.

Fichot, F., Harstad, K., Bellan, J., 1994. Unsteady evaporation and combustion of a drop cluster inside a vortex. Combustion and Flame 98 (1–2), 5–19.

Haywood, R.J., Nafziger, R., Renksizbulut, M., 1989. A detailed examination of gas and liquid phase transient processes in convective droplet evaporation. Trans. ASME J. Heat Transfer 111, 495–502.

Kim, I., Elghobashi, S.E., Sirignano, W.A., 1993. Three-dimensional flow over two spheres placed side by side. J. Fluid Mech 246, 465–488.

Kim, I., Elghobashi, S.E., Sirignano, W.A., 1995. Unsteady flow interactions between an advected cylindrical vortex tube and a spherical particle. J. Fluid Mech 288, 123–155.

Kim, I., Elghobashi, S.E., Sirignano, W.A., 1997. Unsteady flow interactions between a pair of advected cylindrical vortex tubes and a rigid sphere. International Journal of Multiphase Flow 23 (1), 1–23.

Masoudi, M., Sirignano, W.A., 1997. Influence of an advecting vortex on the heat transfer to a liquid droplet. Int. J. Heat Mass Transfer 40 (15), 3663–3673.

Masoudi, M., Sirignano, W.A., 1998. The influence of an advecting vortex on the heat transfer to a translating sphere in a stratified temperature field. Int. J. Heat Mass Transfer 41 (17), 2639–2652.

Masoudi, M., 1998. Droplet heating and vaporization influenced by vortex collision. Ph.D. Dissertation, University of California, Irvine.

Niazmand, H., Shaw, B.D., Dwyer, H.A., Aharon, I., 1994. Effects of Marangoni convection on transient droplet evaporation. Combustion Science and Tech. 103, 219–233.

Reid, R.C., Prausnitz, J.M., Poling, B.E., 1987. The Properties of Gases and Liquids, 4th ed. McGraw-Hill, New York.

Renksizbulut, M., Yuen, M.C., 1983. Numerical study of droplet evaporation in a high-temperature stream. Trans. ASME J. Heat Transfer 105, 389–397.

Saffman, P.G., 1992. Vortex Dynamics. Cambridge University Press, Cambridge.

Shih, A.T., Megaridis, C.M., 1996. Thermocapillary flow effects on convective droplet evaporation. Int. J. Heat Mass Transfer 39, N2:247–257.

Sirignano, W.A., 1983. Fuel droplet vaporization and spray combustion theory. Prog. Energy Combust. Sci 9, 291–322.

Sirignano, W.A., 1999. Fluid Dynamics and Transport of Droplets and Sprays. Cambridge University Press, New York.

Vargaftik, N.B., 1975. Tables on the Thermophysical Properties of Liquids and Gases, 2nd ed. Hemisphere, Washington, DC.